Analysis of Fluid Flow in Axial Re-entrant Grooves with Application to Heat Pipes

Scott K. Thomas[1] and Vikrant C. Damle[2]
Wright State University, Dayton, Ohio 45435

The fully developed laminar flow within a re-entrant groove has been analyzed using a finite element model. Re-entrant grooves have been used in both axially-grooved heat pipes and in monogroove heat pipes. The main benefit to using this type of wick structure is the reduction of the liquid pressure drop along the length of the groove due to countercurrent liquid-vapor interaction at the meniscus. All previous researchers assumed that the pressure drop within the liquid could be modelled as flow within a smooth tube, but the results of the current analysis show that this assumption can lead to significant errors in the pressure drop prediction. An extensive literature survey was completed and the results of five previous studies were used to validate the current numerical model. It was found that the present finite element model is both more accurate and consumes less computer resources than a finite difference based model developed previously by one of the authors of the current manuscript. A parametric analysis was carried out to determine the Poiseuille number, Po = fRe, the dimensionless mean velocity, $\overline{v^*}$, and the dimensionless volumetric flow rate, $\dot{V}^*$, as functions of the geometry of the re-entrant groove (groove height $1.0 \leq H^* \leq 4.0$, slot half-width $0.05 \leq W^*/2 \leq 0.9$, fillet radius $0.0 \leq R_f^* \leq 1.0$), and the liquid-vapor shear stress ($0.0 \leq -\tau_{lv}^* \leq 2.5$). It was determined that the flow variables were strongly affected by the groove height, slot half-width and liquid-vapor shear stress, but were relatively unaffected by the fillet radius. The case in which the meniscus recedes into the re-entrant groove was examined, which could be a result of evaporator dry-out or insufficient liquid fill amount. The cross-sectional area of the liquid in the groove, A_l^*, the meniscus radius, R_m^*, and the above-mentioned flow variables were calculated as functions of the meniscus contact angle ($0^\circ \leq \phi \leq 40^\circ$) and meniscus attachment point ($0.0 \leq H_l^* \leq 2.75$). In general, the flow variables were more strongly affected by the meniscus attachment point than the meniscus contact angle. Finally, the results of the numerical model were used to determine the capillary limit of a low-temperature heat pipe with two different working fluids, water and ethanol, for a range of meniscus contact angles. The capillary limit heat transfer was found to attain a maximum value in the slot region and then decreased dramatically when the meniscus receded into the circular region of the re-entrant groove.

Nomenclature

A_g = total cross-sectional area of the re-entrant groove, m^2
A_g^* = A_g/R^2
A_l = cross-sectional area of the liquid, m^2
A_l^* = A_l/R^2
D_h = hydraulic diameter, $4A_l/P$, m
D_h^* = D_h/R
f = friction coefficient, $2\overline{\tau_w}/\rho\overline{v}^2$
h_{fg} = heat of vaporization, J/kg
H = distance from the center of the circular portion of the re-entrant groove to the top of the slot, m
H^* = H/R

[1]Associate Professor, Department of Mechanical and Materials Engineering AIAA Associate Fellow, corresponding author
[2]Graduate Assistant, Department of Mechanical and Materials Engineering

H_l = vertical location of the attachment point of the meniscus to the re-entrant groove wall, m
H_l^* = H_l/R
$H_{l,s}$ = vertical location of the attachment point of the meniscus to the sinusoidal groove wall, m
H_s = height of the sinusoidal groove, m
H_{tr} = height of the trapezoidal groove, m
K = thermal conductivity, W/(m-K)
L_a = adiabatic length, m
L_c = condenser length, m
L_e = evaporator length, m
L_{eff} = effective heat pipe length, $L_e/2 + L_a + L_c/2$, m
n = coordinate normal to the liquid-vapor interface
n^* = n/R
N_g = number of grooves
p = pressure, N/m^2
P = wetted perimeter, m
P^* = P/R
Po = Poiseuille number, $f\text{Re}$
$q_{lv}^{''}$ = heat flux at the liquid-vapor interface, W/m^2
$q_{lv}^{''*}$ = $q_{lv}^{''}/q^{'''}R$
$q^{'''}$ = internal volumetric heat generation, W/m^3
$\dot{Q}_{\text{cap}}$ = capillary limit heat transport, W
$\dot{Q}_g$ = heat transfer due to a single groove, W
$\dot{Q}_t$ = total heat transported, $N_g\dot{Q}_g$, W
R = radius of the circular portion of the re-entrant groove, m
R_f = radius of the fillet, m
R_f^* = R_f/R
R_m = radius of the meniscus, m
R_m^* = R_m/R
R_v = radius of the heat pipe vapor space, m
Re = Reynolds number, $\rho\overline{v}D_h/\mu$
T = temperature, K
T_{sat} = saturation temperature, K
T^* = $KT/R^2q^{'''}$
v = y-direction velocity, m/s
$\overline{v}$ = mean y-direction velocity, m/s
$\overline{v}_{l,\max}$ = maximum mean liquid velocity, m/s
v^* = $\mu v/R^2(-dp/dy)$
$\overline{v^*}$ = $\mu\overline{v}/R^2(-dp/dy)$
$\dot{V}$ = volumetric flow rate, $\overline{v}A_l$, m^3/s
$\dot{V}^*$ = $\mu\dot{V}/[R^4(-dp/dy)]$
W = width of the slot, m
W^* = W/R
W_l = width of the liquid meniscus at the attachment point to the re-entrant groove wall, m
W_l^* = W_l/R
$W_{l,s}$ = width of the liquid meniscus at the attachment point to the sinusoidal groove wall, m
W_s = width of the sinusoidal groove, m
W_{tr} = width of the trapezoidal groove, m
x, y, z = Cartesian coordinate directions
x^*, y^*, z^* = $x/R, y/R, z/R$
$x_{f,0}, z_{f,0}$ = location of the center point of the circular fillet, m
$x_{f,0}^*$ = $x_{f,0}/R = W^*/2 + R_f^*$
x_t, z_t = point of tangency of the fillet and the circular portion of the re-entrant groove, m
x_t^* = $x_t/R = x_{f,0}^*/\left(1 + R_f^*\right)$

$z^*_{f,0}$ $= z_{f,0}/R = z^*_t - (z^*_t - 1)\left(1 - x^*_{f,0}/x^*_t\right)$
z^*_t $= z_t/R = 1 + \sqrt{1 - x^{*2}_t}$
z_0 = location of the center point of the circular liquid meniscus, m
z^*_0 $= z_0/R$
α = circular segment duct half-angle, rad
β = aspect ratio for the rectangular and trapezoidal grooves, $2H_r/W_r$ or $2H_{tr}/W_{tr}$
γ = triangular groove half-angle, rad
θ = trapezoidal groove half-angle, rad
μ = absolute viscosity, Pa-s
ρ = density, kg/m^3
σ = surface tension, N/m
τ_{lv} = shear stress at the liquid-vapor interface, N/m^2
τ^*_{lv} $= \tau_{lv}/R(-dp/dy)$
$\overline{\tau_w}$ = average shear stress at the wall, N/m^2
ϕ = meniscus contact angle, rad
ϕ_0 = minimum meniscus contact angle, rad
ψ_1 $= \tan^{-1}\left[(W^*_l/2)\,/\,(H^*_l - 1)\right]$
ψ_2 $= \tan^{-1}\left[\left(W^*_l/2 - x^*_{f,0}\right)\,/\,\left(H^*_l - z^*_{f,0}\right)\right]$

I. Introduction

For years, heat pipes have been widely used for thermal control in both terrestrial and space-based applications. Heat pipes provide a high heat transfer rate with approximately isothermal behavior and self-regulating cooling characteristics. For a high heat transfer rate, the capillary structure must be designed in such a way that it combines a high capillary pumping pressure (pressure difference between the liquid and vapor sides of the meniscus) with a low axial pressure drop in the liquid. The first aim can be achieved by using small rectangular, trapezoidal, or triangular grooves. However, these structures lead to a relatively high axial pressure drop in the liquid and, therefore, the second aim cannot be fulfilled. Harwell et al. [1] described the heat transfer characteristics of an axially-grooved aluminum extrusion with a re-entrant groove profile. A typical cross section for this type of heat pipe is shown in Fig. 1(a). This configuration combines a high capillary pumping pressure with a low axial pressure drop in the liquid (Dubois et al. [2], [3]). In addition, the retardation of the liquid flow due to the countercurrent vapor flow over the liquid-vapor interface is minimized as compared to other axial groove designs. However, the radial thermal resistance to heat transfer of the re-entrant groove geometry may be larger compared to rectangular, trapezoidal, or triangular groove designs due to an increase in the wall thickness of the heat pipe.

The monogroove heat pipe developed by Alario et al. [4] and Alario [5] is an aluminum extrusion with a single slot connecting the vapor channel to the liquid artery, as shown in Fig. 1(b). In general, axially-grooved heat pipes utilize a relatively large number of small grooves as a compromise between axial transport capacity and radial heat-transfer efficiency. In the monogroove design, the single re-entrant groove is made up of the slot and the liquid artery, which returns the liquid to the evaporator section using the capillary pumping pressure generated by the meniscus residing in the slot. Circumferential grooves on the inside wall in the vapor space provide a means for liquid communication between the vapor space and the re-entrant groove (Henson [6], Brown et al. [7], Schlitt [8]). This geometry combines the advantages of a large axial artery (low pressure drop in the liquid) with large areas for evaporation and condensation on the circumferential wall grooves. In addition, the heat input is removed as far as possible from the liquid artery, which reduces the possibility of boiling within the liquid artery, which would cause the artery to deprime. A disadvantage of the monogroove heat pipe is related to the narrow slot width, which is necessary for a high capillary pumping pressure within the slot. This causes the liquid fill amount inside the liquid channel to be so critical that a small decrease in liquid fill may result in a significant decrease in the capillary pumping pressure and hence a significant decrease in the maximum heat transport.

Previous researchers (e.g., Harwell et al. [1], Alario et al. [4], Henson [6], Brandt et al. [9]) have modelled the flow of liquid in both re-entrant groove heat pipes and in monogroove heat pipes as a one-dimensional laminar flow through a smooth-walled tube in order to determine the pressure drop (Po = fRe = 16). In

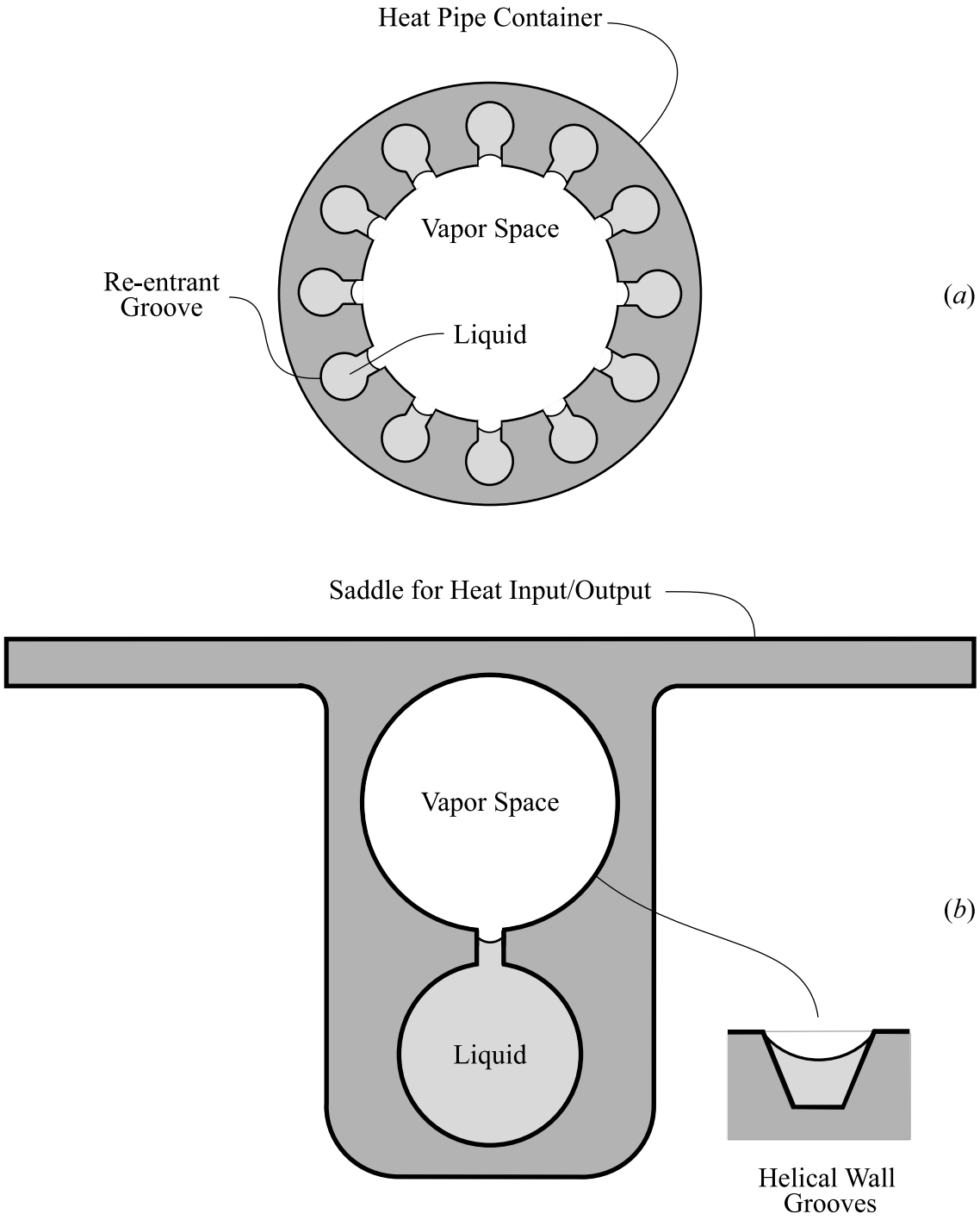

Figure 1: Heat pipes using re-entrant grooves: (a) Multiple re-entrant grooves distributed uniformly around the circumference; (b) Monogroove heat pipe design with a single re-entrant groove.

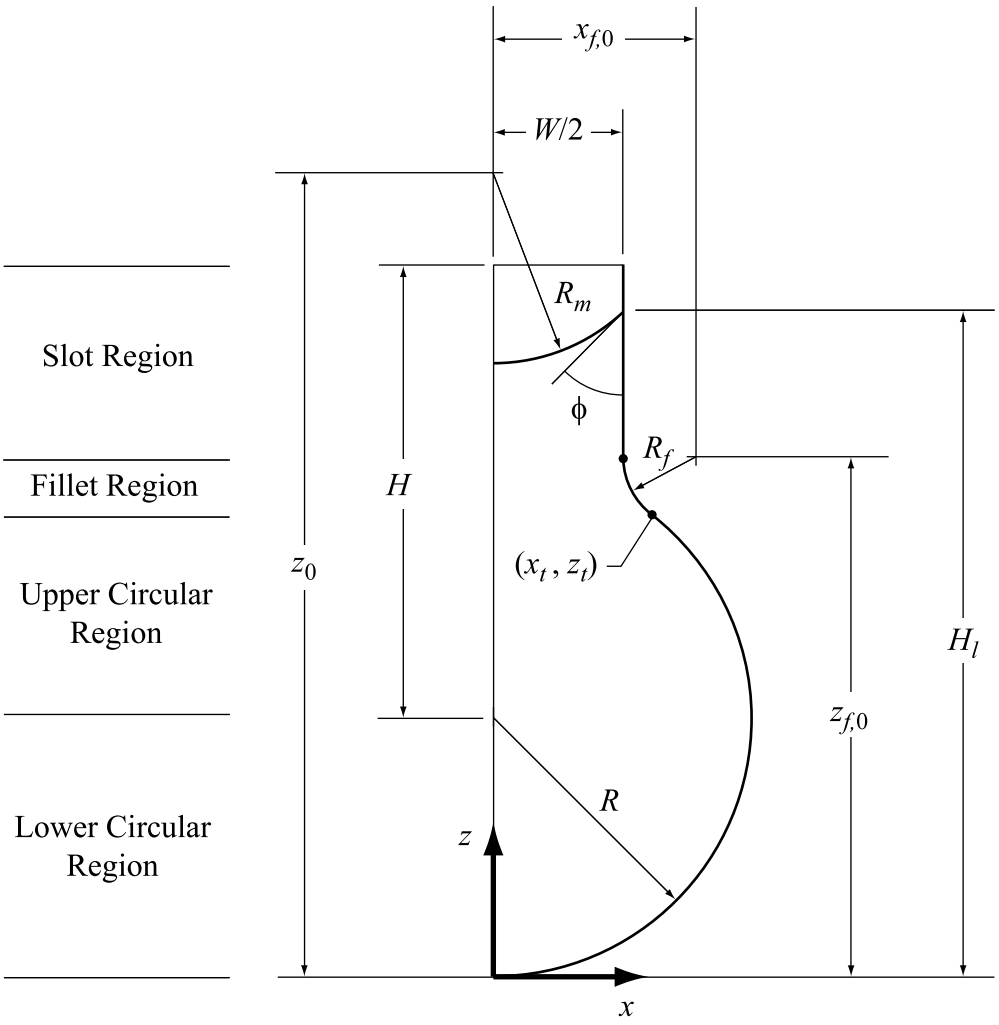

Figure 2: Geometric parameters defining the flow of liquid in a re-entrant groove.

addition, the effect of the shear stress at the liquid-vapor interface has not been accounted for. While Brandt et al. [9] examined the effect of the liquid fill amount in the groove on the capillary pressure, only the case in which the liquid meniscus remained attached to the top of the slot was examined. The present study has addressed these shortcomings by numerically solving the conservation of mass and momentum equations for laminar fully-developed flow in re-entrant grooves with an applied shear stress at the liquid-vapor interface. The meniscus contact angle, countercurrent shear stress at the liquid-vapor interface and groove geometry were varied, and the mean velocity, Poiseuille number and volumetric flow rate have been determined. The results of the numerical model were used in an analytical model of a heat pipe with axial re-entrant grooves. The capillary limit was determined as a function of the minimum meniscus contact angle, groove fill amount and the working fluid.

II. Mathematical Model

A constant property liquid flows steadily in a re-entrant groove as shown in Fig. 2. A meniscus, which is assumed to be circular, comprises the liquid-vapor interface. For fully developed laminar flow with no body forces, the dimensionless conservation of mass and momentum equations reduce to (White [10])

$$\frac{\partial^2 v^*}{\partial x^{*2}} + \frac{\partial^2 v^*}{\partial z^{*2}} = -1 \tag{1}$$

On the groove wall, the no-slip condition is in effect.

$$v^* = 0: \quad x^* = \begin{cases} \sqrt{z^*(2-z^*)}, & 0 \le z^* \le z_t^* \quad \text{(Circular Region)} \\ x_{f,0}^* - \sqrt{R_f^{*2} - \left(z^* - z_{f,0}^*\right)^2}, & z_t^* \le z^* \le z_{f,0}^* \quad \text{(Fillet Region)} \\ W^*/2, & z_{f,0}^* \le z^* \le 1 + H^* \quad \text{(Slot Region)} \end{cases} \tag{2}$$

At the line of symmetry, the velocity gradient is zero in the x^* direction

$$\frac{\partial v^*}{\partial x^*} = 0: \quad x^* = 0, \quad 0 \le z^* \le 1 + H^* \tag{3}$$

At the liquid-vapor interface, a uniform shear stress due to vapor flowing above the meniscus is imposed in the y direction.

$$\frac{\partial v^*}{\partial n^*} = \tau_{lv}^* \tag{4}$$

The dimensional liquid-vapor interfacial shear stress can be cast in terms of the friction factor of the vapor.

$$\tau_{lv} = \begin{cases} \left[\dfrac{\rho_v \left(\overline{v_v}\right)^2}{2}\right] f_v & \text{for cocurrent flow} \\ -\left[\dfrac{\rho_v \left(\overline{v_v}\right)^2}{2}\right] f_v & \text{for countercurrent flow} \end{cases} \tag{5}$$

The equation of the circular liquid meniscus is

$$x^* = \sqrt{R_m^{*2} - \left(z^* - z_0^*\right)^2} \tag{6}$$

The vertical range of this equation depends upon the location of the attachment point of the meniscus to the groove wall.

For $H_l^* \le 1$ (Lower Circular Region):

$$\begin{array}{ll} z_0^* - R_m^* \le z^* \le H_l^* & \text{if } \phi < -\psi_1 \\ H_l^* \le z^* \le z_0^* + R_m^* & \text{if } \phi > -\psi_1 \end{array} \tag{7}$$

For $H_l^* \ge 1$ (Upper Circular Region, Fillet Region and Slot Region):

$$z_0^* - R_m^* \le z^* \le H_l^* \tag{8}$$

The radius, half-width and vertical location of the center point of the circular liquid meniscus are given below.

$$R_m^* = \sqrt{\left(\frac{W_l^*}{2}\right)^2 + \left(H_l^* - z_0^*\right)^2} \tag{9}$$

$$\frac{W_l^*}{2} = \begin{cases} \sqrt{H_l^*(2 - H_l^*)}, & 0 \le H_l^* \le z_t^* \quad \text{(Circular Region)} \\ x_{f,0}^* - \sqrt{R_f^{*2} - \left(H_l^* - z_{f,0}^*\right)^2}, & z_t^* \le H_l^* \le z_{f,0}^* \quad \text{(Fillet Region)} \\ W^*/2, & z_{f,0}^* \le H_l^* \le 1 + H^* \quad \text{(Slot Region)} \end{cases} \tag{10}$$

$$z_0^* = \begin{cases} H_l^* - \dfrac{(W_l^*/2)}{\tan(\phi + \psi_1)}, & 0 \le H_l^* \le z_t^* \quad \text{(Circular Region)} \\ H_l^* - \dfrac{(W_l^*/2)}{\tan(\phi + \psi_2)}, & z_t^* \le H_l^* \le z_{f,0}^* \quad \text{(Fillet Region)} \\ H_l^* + \left(\dfrac{W_l^*}{2}\right)\tan\phi, & z_{f,0}^* \le H_l^* \le 1 + H^* \quad \text{(Slot Region)} \end{cases} \tag{11}$$

The Poiseuille number of the liquid in the groove is given by

$$\mathrm{Po} = f\mathrm{Re} = \frac{D_h^{*2}}{2\overline{v^*}} \tag{12}$$

The mean velocity is defined as

$$\overline{v^*} = \frac{2}{A_l^*}\int_0^{x^*}\int_0^{z^*} v^*\, dz^*\, dx^* \tag{13}$$

The dimensionless hydraulic diameter is

$$D_h^* = \frac{4A_l^*}{P^*} \tag{14}$$

The cross-sectional area of the liquid is given in terms of the meniscus attachment point.

For $0 \le H_l^* \le 1$ (Lower Circular Region):

$$\begin{aligned} A_l^* = {} & \left(\frac{W_l^*}{2}\right)\left[2z_0^* - \sqrt{R_m^{*2} - \left(\frac{W_l^*}{2}\right)^2}\right] - R_m^{*2}\sin^{-1}\left(\frac{W_l^*/2}{R_m^*}\right) \\ & - \left\{\left(\frac{W_l^*}{2}\right)\left[2 - \sqrt{1 - \left(\frac{W_l^*}{2}\right)^2}\right] - \sin^{-1}\left(\frac{W_l^*}{2}\right)\right\} \quad \text{for} \quad \phi < -\psi_1 \end{aligned} \tag{15}$$

$$\begin{aligned} A_l^* = {} & \left(\frac{W_l^*}{2}\right)\left[2z_0^* + \sqrt{R_m^{*2} - \left(\frac{W_l^*}{2}\right)^2}\right] + R_m^{*2}\sin^{-1}\left(\frac{W_l^*/2}{R_m^*}\right) \\ & - \left\{\left(\frac{W_l^*}{2}\right)\left[2 - \sqrt{1 - \left(\frac{W_l^*}{2}\right)^2}\right] - \sin^{-1}\left(\frac{W_l^*}{2}\right)\right\} \quad \text{for} \quad \phi \ge -\psi_1 \end{aligned} \tag{16}$$

For $1 \le H_l^* \le z_t^*$ (Upper Circular Region):

$$\begin{aligned} A_l^* = {} & \pi + \left(\frac{W_l^*}{2}\right)\left[2\left(H_l^* - 1\right) - \sqrt{1 - \left(\frac{W_l^*}{2}\right)^2}\right] - \sin^{-1}\left(\frac{W_l^*}{2}\right) \\ & + R_m^{*2}\left[\cos^{-1}\left(\frac{H_l^* - z_0^*}{R_m^*}\right) - \pi\right] - \left(H_l^* - z_0^*\right)\sqrt{R_m^{*2} - \left(H_l^* - z_0^*\right)^2} \quad \text{for} \quad \phi < \frac{\pi}{2} - \psi_1 \end{aligned} \tag{17}$$

$$\begin{aligned} A_l^* = {} & \pi + \left(\frac{W_l^*}{2}\right)\left[2z_0^* - \sqrt{R_m^{*2} - \left(\frac{W_l^*}{2}\right)^2}\right] - R_m^{*2}\sin^{-1}\left(\frac{W_l^*/2}{R_m^*}\right) \\ & - \left\{\left(\frac{W_l^*}{2}\right)\left[2 + \sqrt{1 - \left(\frac{W_l^*}{2}\right)^2}\right] + \sin^{-1}\left(\frac{W_l^*}{2}\right)\right\} \quad \text{for} \quad \phi \ge \frac{\pi}{2} - \psi_1 \end{aligned} \tag{18}$$

For $z_t^* \le H_l^* \le z_{f,0}^*$ (Fillet Region):

$$\begin{aligned} A_l^* = {} & \pi + W_l^* H_l^* + \left(x_t^* - x_{f,0}^*\right)\left[2z_{f,0}^* - \sqrt{R_f^{*2} - \left(x_t^* - x_{f,0}^*\right)^2}\right] \\ & - \left(\frac{W_l^*}{2} - x_{f,0}^*\right)\left[2z_{f,0}^* - \sqrt{R_f^{*2} - \left(\frac{W_l^*}{2} - x_{f,0}^*\right)^2}\right] \\ & - R_f^{*2}\left[\sin^{-1}\left(\frac{x_t^* - x_{f,0}^*}{R_f^*}\right) - \sin^{-1}\left(\frac{W_l^*/2 - x_{f,0}^*}{R_f^*}\right)\right] \\ & - x_t^*\left(2 + \sqrt{1 - x_t^{*2}}\right) - \sin^{-1}\left(x_t^*\right) + R_m^{*2}\left[\cos^{-1}\left(\frac{H_l^* - z_0^*}{R_m^*}\right) - \pi\right] \\ & - \left(H_l^* - z_0^*\right)\sqrt{R_m^{*2} - \left(H_l^* - z_0^*\right)^2} \quad \text{for} \quad \phi < \frac{\pi}{2} - \psi_2 \end{aligned} \tag{19}$$

$$\begin{aligned} A_l^* = {} & \pi + \left(\frac{W_l^*}{2}\right)\left[2z_0^* - \sqrt{R_m^{*2} - \left(\frac{W_l^*}{2}\right)^2}\right] - R_m^{*2}\sin^{-1}\left(\frac{W_l^*/2}{R_m^*}\right) \\ & + \left(x_t^* - x_{f,0}^*\right)\left[2z_{f,0}^* - \sqrt{R_f^{*2} - \left(x_t^* - x_{f,0}^*\right)^2}\right] \\ & - \left(\frac{W_l^*}{2} - x_{f,0}^*\right)\left[2z_{f,0}^* - \sqrt{R_f^{*2} - \left(\frac{W_l^*}{2} - x_{f,0}^*\right)^2}\right] \\ & - R_f^{*2}\left[\sin^{-1}\left(\frac{x_t^* - x_{f,0}^*}{R_f^*}\right) - \sin^{-1}\left(\frac{W_l^*/2 - x_{f,0}^*}{R_f^*}\right)\right] \\ & - x_t^*\left(2 + \sqrt{1 - x_t^{*2}}\right) - \sin^{-1}\left(x_t^*\right) \quad \text{for} \quad \phi \ge \frac{\pi}{2} - \psi_2 \end{aligned} \tag{20}$$

For $z_{f,0}^* \le H_l^* \le 1 + H^*$ (Slot Region):

$$\begin{aligned} A_l^* = {} & \pi + \left(\frac{W_l^*}{2}\right)\left[2z_0^* - \sqrt{R_m^{*2} - \left(\frac{W_l^*}{2}\right)^2}\right] - R_m^{*2}\sin^{-1}\left(\frac{W_l^*/2}{R_m^*}\right) \\ & + \left(x_t^* - x_{f,0}^*\right)\left[2z_{f,0}^* - \sqrt{R_f^{*2} - \left(x_t^* - x_{f,0}^*\right)^2}\right] \\ & + 2R_f^* z_{f,0}^* - R_f^{*2}\left[\sin^{-1}\left(\frac{x_t^* - x_{f,0}^*}{R_f^*}\right) + \frac{\pi}{2}\right] - x_t^*\left(2 + \sqrt{1 - x_t^{*2}}\right) - \sin^{-1}\left(x_t^*\right) \end{aligned} \tag{21}$$

The total cross-sectional area of the re-entrant groove is

$$\begin{aligned} A_g^* = {} & \pi + W^*\left(1 + H^*\right) + \left(x_t^* - x_{f,0}^*\right)\left[2z_{f,0}^* - \sqrt{R_f^{*2} - \left(x_t^* - x_{f,0}^*\right)^2}\right] \\ & + 2R_f^* z_{f,0}^* - R_f^{*2}\left[\sin^{-1}\left(\frac{x_t^* - x_{f,0}^*}{R_f^*}\right) + \frac{\pi}{2}\right] - x_t^*\left(2 + \sqrt{1 - x_t^{*2}}\right) - \sin^{-1}\left(x_t^*\right) \end{aligned} \tag{22}$$

The wetted perimeter is also given in terms of the location of the attachment point of the meniscus. For $0 \le H_l^* \le z_t^*$ (Circular Region):

$$P^* = \pi + 2\tan^{-1}\left(\frac{H_l^* - 1}{W_l^*/2}\right) \tag{23}$$

For $z_t^* \le H_l^* \le z_{f,0}^*$ (Fillet Region):

$$P^* = \pi + 2\tan^{-1}\left(\frac{z_t^* - 1}{x_t^*}\right) + 2R_f^*\left[\tan^{-1}\left(\frac{W_l^*/2 - x_{f,0}^*}{H_l^* - z_{f,0}^*}\right) - \tan^{-1}\left(\frac{x_t^* - x_{f,0}^*}{z_t^* - z_{f,0}^*}\right)\right] \tag{24}$$

For $z_{f,0}^* \le H_l^* \le 1 + H^*$ (Slot Region):

$$P^* = \pi + 2\tan^{-1}\left(\frac{z_t^* - 1}{x_t^*}\right) + 2R_f^*\left[\frac{\pi}{2} - \tan^{-1}\left(\frac{x_t^* - x_{f,0}^*}{z_t^* - z_{f,0}^*}\right)\right] + 2\left(H_l^* - z_{f,0}^*\right) \tag{25}$$

III. Numerical Model Validation

The finite-element code available to the researchers could solve the elliptic Poisson equation [eqn. (1)] with mixed boundary conditions [eqns. (2)-(4)] by using a simple transformation. The fluid flow problem was solved as a heat conduction problem by mapping the variables, geometry and boundary conditions. The analogous steady state heat conduction problem is one in which a plate of uniform thickness and constant properties has a uniform internal volumetric heat generation. The conservation of energy equation for this case is given below in dimensionless form (Incropera and DeWitt [11]).

$$\frac{\partial^2 T^*}{\partial x^{*2}} + \frac{\partial^2 T^*}{\partial z^{*2}} = -1 \tag{26}$$

The boundary conditions for the energy equation must also match those of the fluid flow problem. The temperature on the groove wall is zero.

$$T^* = 0: \quad x^* = \begin{cases} \sqrt{z^*(2 - z^*)}, & 0 \le z^* \le z_t^* \quad \text{(Circular Region)} \\ x_{f,0}^* - \sqrt{R_f^{*2} - \left(z^* - z_{f,0}^*\right)^2}, & z_t^* \le z^* \le z_{f,0}^* \quad \text{(Fillet Region)} \\ W^*/2, & z_{f,0}^* \le z^* \le 1 + H^* \quad \text{(Slot Region)} \end{cases} \tag{27}$$

At the line of symmetry, the heat flux is zero in the x^* direction

$$\frac{\partial T^*}{\partial x^*} = 0: \quad x^* = 0, \quad 0 \le z^* \le 1 + H^* \tag{28}$$

The dimensionless heat flux at the liquid-vapor interface is specified.

$$\frac{\partial T^*}{\partial n^*} = -q_{lv}^{''*} \tag{29}$$

The elliptic Poisson equation given by eqn. (26) with mixed boundary conditions [eqns. (27)-(29)] was solved using a finite element code. The solution was considered to be independent of the number of elements when the Poiseuille number changed by less than 1% when the number of elements was doubled.

The numerical model was tested against existing solutions for a variety of situations to ensure the validity of the results (see Damle [12]). Shah and London [13] determined the friction factors for the laminar flow within a family of circular segment ducts using a least-squares-matching technique. A comparison of the Poiseuille number between the present solution and that given by Shah and London [13] for $8^\circ \le 2\alpha \le 160^\circ$ was made, and the agreement was excellent with a maximum difference of 1.4%.

DiCola [14] solved the conservation of mass and momentum equations for the laminar flow of liquid in rectangular grooves with a uniform shear stress imposed at the liquid-vapor interface using separation of variables. The comparison of the Poiseuille number for the present solution and the solution given by DiCola [14] for $\tau_{lv}^* = -0.1$, 0 and 1.0 and $0.1 \le \beta \le 1.0$ resulted in a maximum difference of 1.2%.

Romero and Yost [15] analyzed the flow of liquid in a triangular groove with no shear stress at the liquid-vapor interface. The present solution was compared with that provided by Romero and Yost [15] for $\gamma = 5^\circ$ and 60° and $0.1^\circ \le \phi \le 80^\circ$, which resulted in a maximum difference of 2.6%.

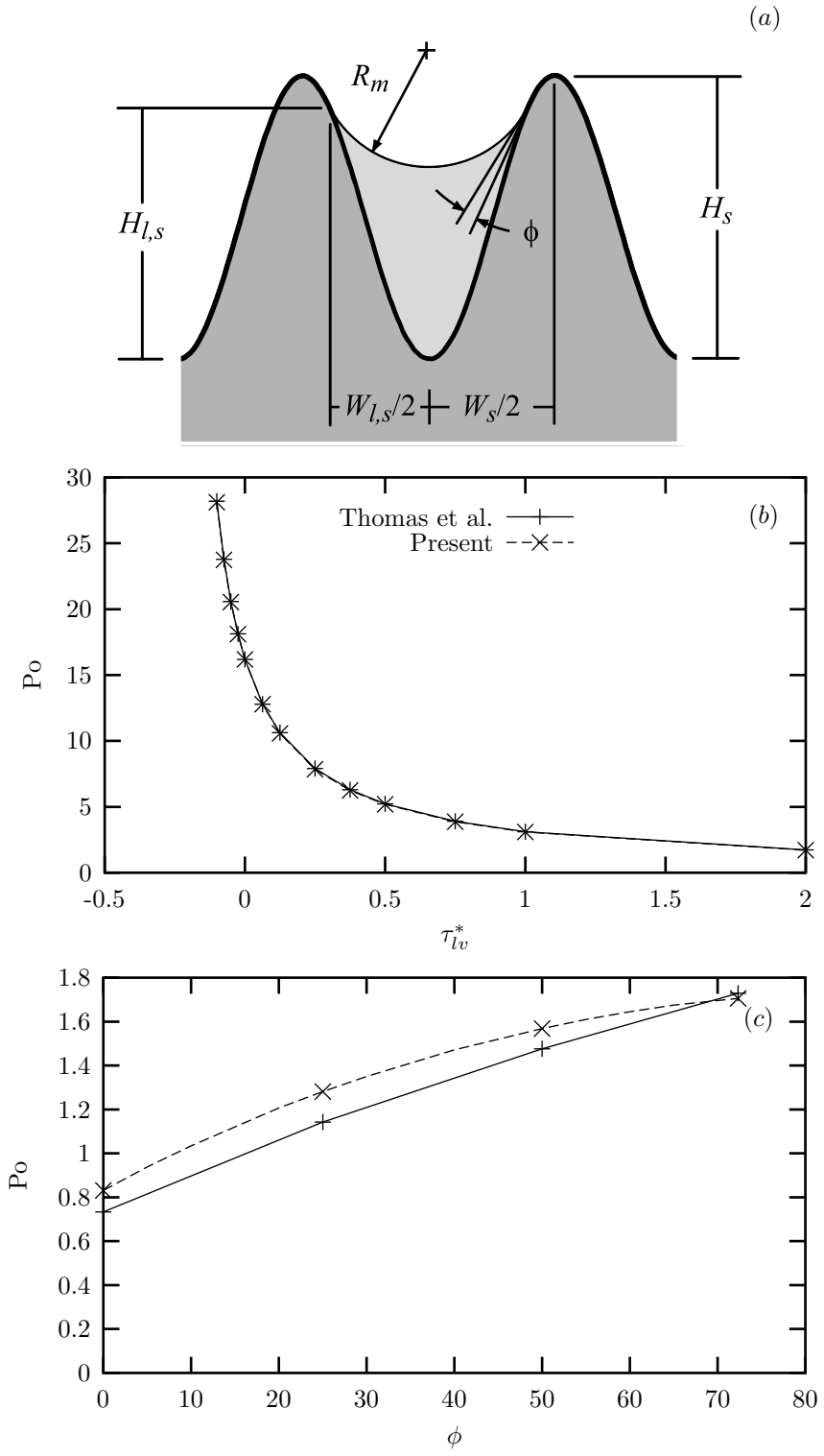

Figure 3: Comparison of the present solution with that given by Thomas et al. [16] for the sinusoidal groove ($\beta = 0.5$, $W^*_{l,s}/2 = 0.25$, $P^* = 1.15245$): (a) Sinusoidal groove geometry; (b) Poiseuille number versus liquid-vapor shear stress ($\phi = 72.34°$); (c) Poiseuille number versus meniscus contact angle ($\tau^*_{lv} = 2.0$).

Thomas et al. [16] and [17] solved the elliptic Poisson equation with mixed boundary conditions using Gauss-Seidel iteration with successive over-relaxation for sinusoidal and trapezoidal grooves, respectively. The results of the present solution for sinusoidal grooves are compared with those given by Thomas et al. [16] in Fig. 3 for $\phi = 0°$, $25°$, $50°$, and $72.34°$ and $-0.1 \leq \tau^*_{lv} \leq 2.0$. The present numerical model was also compared to that given by Thomas et al. [17] for trapezoidal grooves as shown in Fig. 4 for $\phi = 0°$, $20°$, $40°$, and $60°$ and $-0.375 \leq \tau^*_{lv} \leq 5.0$. Due to the rectangular nature of the grid used to solve the Poisson equation, the shear stress boundary condition at the liquid-vapor interface given by eqn. (4) was approximated by Thomas et al. [16] and [17] as follows.

$$\frac{\partial v^*}{\partial n^*} \simeq \frac{\partial v^*}{\partial z^*} = \tau^*_{lv} \tag{30}$$

In other words, the shear stress was not applied normally to the liquid-vapor interface except when the interface was parallel to the x^* axis. In the present analysis, it was possible to apply the shear stress normally to the liquid surface using the finite element code. This caused a significant difference between the present analysis and those given by Thomas et al. [16] and [17]. When the liquid surface was flat, i.e., when the meniscus contact angle was $\phi = 72.34°$ for the sinusoidal groove (Fig. 3(b)) and $\phi = 60°$ for the trapezoidal groove (Fig. 4(b)), the results of the present analysis and the results obtained by Thomas et al. [16] and [17] were in agreement with a maximum difference 1.4% for the sinusoidal groove and 1.4% for the trapezoidal groove. As the meniscus contact angle decreased, the difference between the present results and those by Thomas et al. [16] and [17] differed by as much as 14%, as shown in Figs. 3(c) and 4(c). This illustrates that the shear stress approximation considered by Thomas et al. [16] and [17] was the cause of the difference in the results.

IV. Results and Discussion

A. Parametric Analysis

A numerical study has been completed in which the flow field in a re-entrant groove has been solved. Specifically, the mean velocity, Poiseuille number, and volumetric flow rate are reported for various values of the dimensionless shear stress at the liquid-vapor interface, groove height, slot width, and fillet radius. Figure 5 shows the dimensionless velocity in a typical re-entrant groove with and without countercurrent shear stress at the free surface. For $\tau^*_{lv} = 0.0$, Fig. 5(a), the maximum velocity is located slightly above the center of the circular region. In Fig. 5(b), where a countercurrent shear stress ($\tau^*_{lv} = -2.5$) is imposed on the liquid-vapor interface, the velocity is maximum inside the circular region and is decreasing in the slot region. Due to the magnitude of the countercurrent shear at the liquid-vapor interface, the liquid near the meniscus was forced in the direction opposite to the pressure gradient.

The mean velocity, Poiseuille number, and the volumetric flow rate versus the liquid-vapor shear stress are shown in Fig. 6. The mean velocity is linear with countercurrent liquid-vapor shear stress as discussed by Thomas et al. [16]. An increase in the shear stress offers more resistance to the fluid flow, which causes the mean velocity to decrease. The Poiseuille number increases monotonically with liquid-vapor shear stress as expected, since the Poiseuille number is inversely proportional to the mean velocity. The Poiseuille number increases dramatically with liquid-vapor shear stress for $H^* \leq 1.5$. This occurs because the liquid-vapor interface is much closer to the circular region, and therefore the effect of the shear stress penetrates into the circular region more profoundly. Also, the volumetric flow rate decreases with an increase in shear stress, which is due to the decrease in mean velocity.

The variation of the three flow variables with the slot height is given in Fig. 7 for $\tau^*_{lv} = 0.0$. The mean velocity is a weak function of H^* for the range of slot half-width studied here, and is nearly constant for $W^*/2 \leq 0.5$. The Poiseuille number approaches the limiting value of Po = 16 (circular duct) as the groove height $H^* \to 1$ and as the slot width $W^*/2 \to 0$ as expected. The mean velocity, Poiseuille number and volumetric flow rate are affected by the slot width more significantly when the groove height is larger. For slot widths less than $W^*/2 \leq 0.3$, the volumetric flow rate does not change significantly, regardless of groove height. Since the area and mean velocity increase with both H^* and $W^*/2$, the volumetric flow rate increases in proportion.

The effect of slot width is shown in Fig. 8. The mean velocity, Poiseuille number and volumetric flow rate are affected by the slot width more significantly as the groove height increases. The Poiseuille number

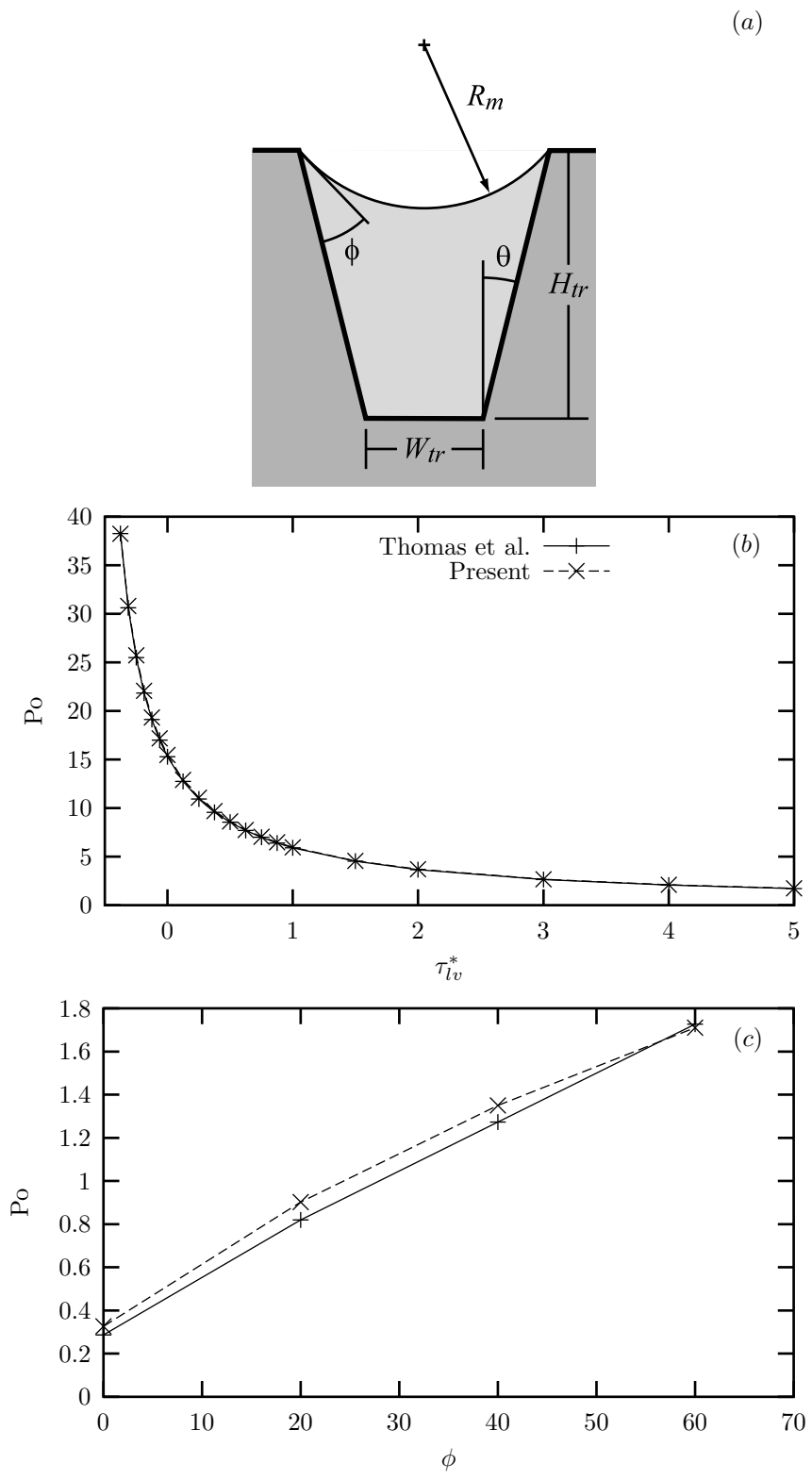

Figure 4: Comparison of the present solution with that given by Thomas et al. [17] for the trapezoidal groove ($\beta = 1.0$, $\theta = 30°$): (a) Trapezoidal groove geometry; (b) Poiseuille number versus liquid-vapor shear stress ($\phi = 60°$); (c) Poiseuille number versus meniscus contact angle ($\tau^*_{lv} = 5.0$).

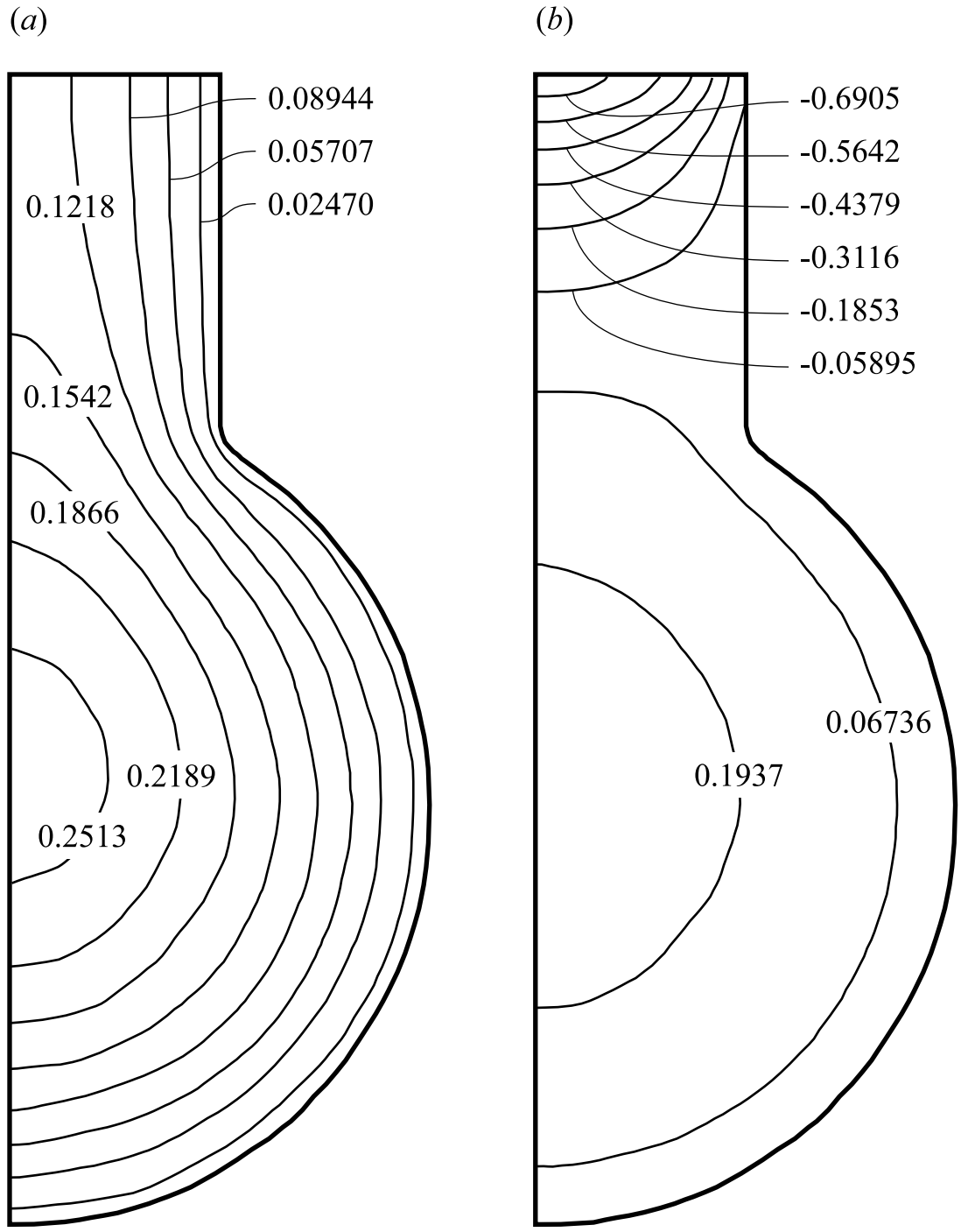

Figure 5: Dimensionless velocity fields for laminar flow in a re-entrant groove ($H^* = 1.75$, $H_l^* = 2.75$, $W^*/2 = 0.5$, $\phi = 90°$: (*a*) $\tau_{lv}^* = 0.0$; (*b*) $\tau_{lv}^* = -2.5$.

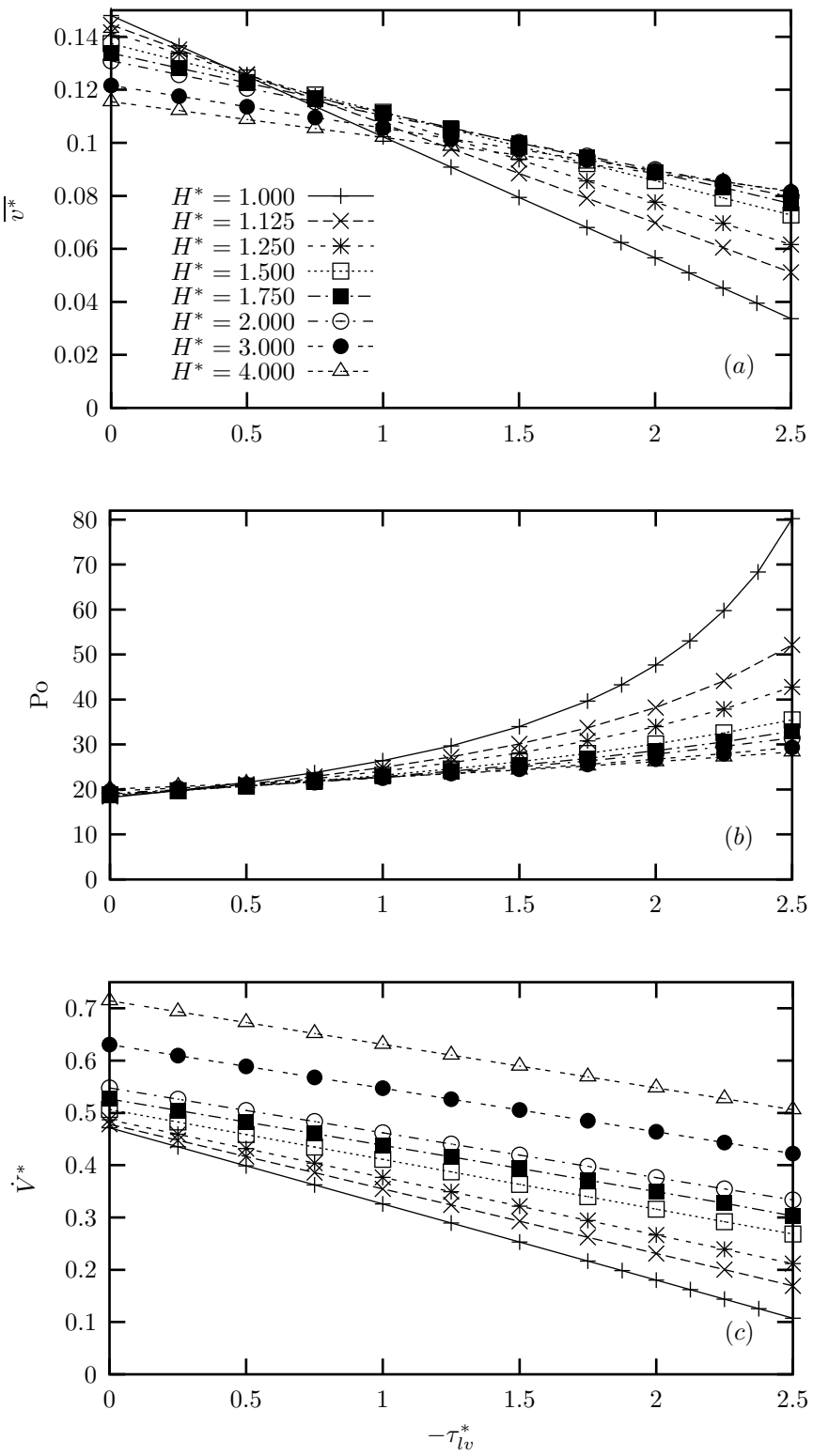

Figure 6: Variation of the flow variables with countercurrent shear stress at the liquid-vapor interface ($\phi = 90°$, $W^*/2 = 0.5$, $R^*_f = 0.1$, $H^*_l = H^* + 1$): (a) Mean velocity; (b) Poiseuille number; (c) Volumetric flow rate.

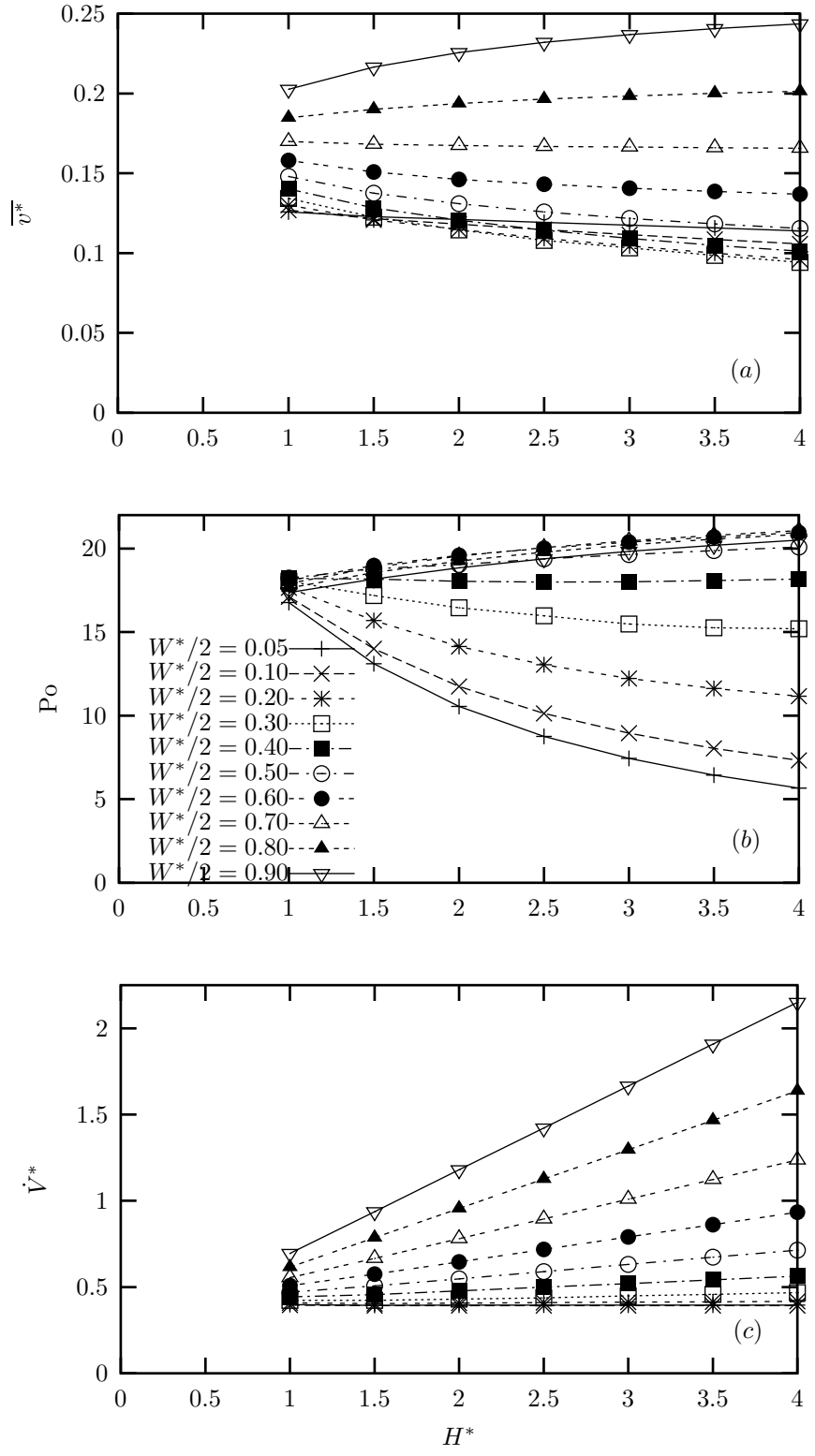

Figure 7: Variation of the flow variables with groove height ($\phi = 90°$, $R_f^* = 0.1$, $H_l^* = H^* + 1$, $\tau_{lv}^* = 0.0$): (a) Mean velocity; (b) Poiseuille number; (c) Volumetric flow rate.

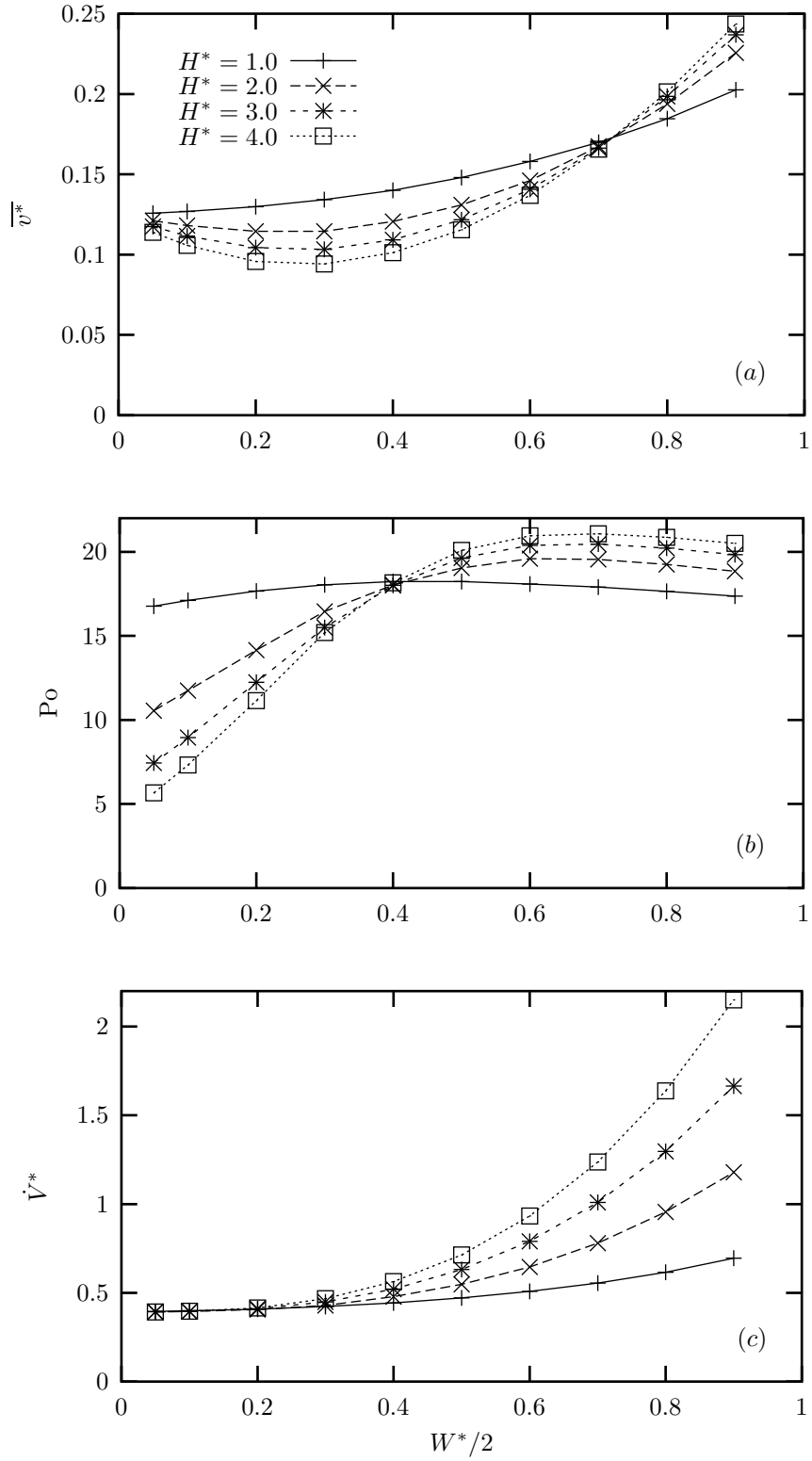

Figure 8: Variation of the flow variables with slot width ($\phi = 90°$, $R_f^* = 0.1$, $H_l^* = H^* + 1$, $\tau_{lv}^* = 0.0$): (a) Mean velocity; (b) Poiseuille number; (c) Volumetric flow rate.

increases substantially with slot width for $W^*/2 \leq 0.4$, and then becomes relatively constant. The volumetric flow rate is a monotonic function of slot width, but is nearly constant for $W^*/2 \leq 0.3$ for all values of groove height studied here. This is of interest for the monogroove-style of heat pipe, wherein the slot width is very small in comparison to the circular portion of the groove.

The effect of the fillet radius was investigated as shown to scale in Fig. 9. The variation of the flow variables with the fillet radius over a range of slot widths is presented in Fig. 10. In general, the mean velocity, Poiseuille number and volumetric flow rate are very weak functions of the fillet radius due to the small change in liquid area with fillet radius.

B. Effect of Groove Fill Amount

The dimensions of the grooves analyzed by Brandt et al. [9] were used to determine the mean velocity, volumetric flow rate and Poiseuille number of liquid flowing in a re-entrant groove as a function of the amount of liquid in the groove. Faghri [18] gives values of the minimum meniscus contact angle for a receding meniscus for various liquids in contact with metal walls. Since the range for ϕ_0 given by Faghri is fairly large, the minimum meniscus contact angle was varied from $\phi_0 = 0°$ to 40°.

Figure 11(a) shows the case when liquid evaporates from a re-entrant groove with $\phi_0 = 10°$. Initially, the groove is full with $\phi = 90°$. The contact angle decreases until the minimum meniscus contact angle ϕ_0 for the particular solid-liquid combination is reached. Past this point, the meniscus detaches from the top of the groove and recedes into the groove (Hopkins et al. [19]). When the meniscus reaches the fillet region of the groove, the cross-sectional area decreases dramatically for small changes in the height of the meniscus attachment point due to the requirement that the contact angle must remain constant, as shown in Fig. 12(a). The decrease in liquid area is more significant in the fillet and circular regions of the groove for smaller values of ϕ_0. In fact, the liquid area $A_l^* \to 0$ when $H_l^* \to z_t^*$ for $\phi_0 = 0°$, since the meniscus radius equals the wall radius for this case. The meniscus radius is shown as a function of the meniscus attachment point in Fig. 12(b). During the meniscus recession process, after the minimum meniscus contact angle has been reached, R_m^* is constant in the slot region. In the fillet region, however, the meniscus radius may increase or decrease as the meniscus recedes further into the re-entrant groove depending on ϕ_0. In all cases, as the meniscus continues to recede into the circular region, the meniscus radius increases dramatically. In the lower circular region shown in Fig. 11, the radius of curvature may approach infinity depending on the minimum meniscus contact angle and the attachment point of the meniscus to the groove wall. Past this point, the liquid in the groove can become convex instead of concave, as shown in Fig. 11(b).

The flow variables versus the meniscus attachment point are presented in Fig. 13. As the liquid recedes into the groove, the mean velocity increases, attains a maximum and then decreases to zero. The minimum meniscus contact angle does not affect the mean velocity significantly until the meniscus reaches the upper circular region, as shown in Fig. 13(a). In Fig. 13(b), the Poiseuille number is relatively constant in the slot region for a given meniscus contact angle, and then decreases in the fillet region due to the sharp decrease in the liquid cross-sectional area. This point can be seen by recasting the Poiseuille number in terms of the liquid area by combining eqns. (12) and (14).

$$\mathrm{Po} = \frac{8A_l^{*2}}{P^*\overline{v^*}} \tag{31}$$

The volumetric flow rate is shown in Fig. 13(c), where the flow rate decreases steadily in the slot region, and then decreases very quickly in the fillet region, which follows the trend in the mean velocity. The flow variables are also presented in Fig. 14 versus the groove fill amount. Interestingly, the dimensionless volumetric flow rate for all of the meniscus contact angles studied here nearly collapse to a single curve.

C. Capillary Limit Analysis for a Heat Pipe using Axial Re-entrant Grooves

Using the results of the numerical analysis, the capillary limit prediction for a heat pipe with re-entrant grooves is proposed. The objective is to use the results of the analysis on the effect of groove fill amount to determine the sensitivity of the performance of the heat pipe with groove fill and minimum meniscus contact angle. It is assumed that no body forces act on the liquid in the grooves, the radius of the liquid meniscus is constant along the length of the groove, and the liquid-vapor shear stress is negligible.

A pressure balance within the heat pipe results in the following expression for the capillary limit (Faghri [18], Chi [20])

$$\Delta p_{\mathrm{cap,max}} \geq \Delta p_v + \Delta p_l \tag{32}$$

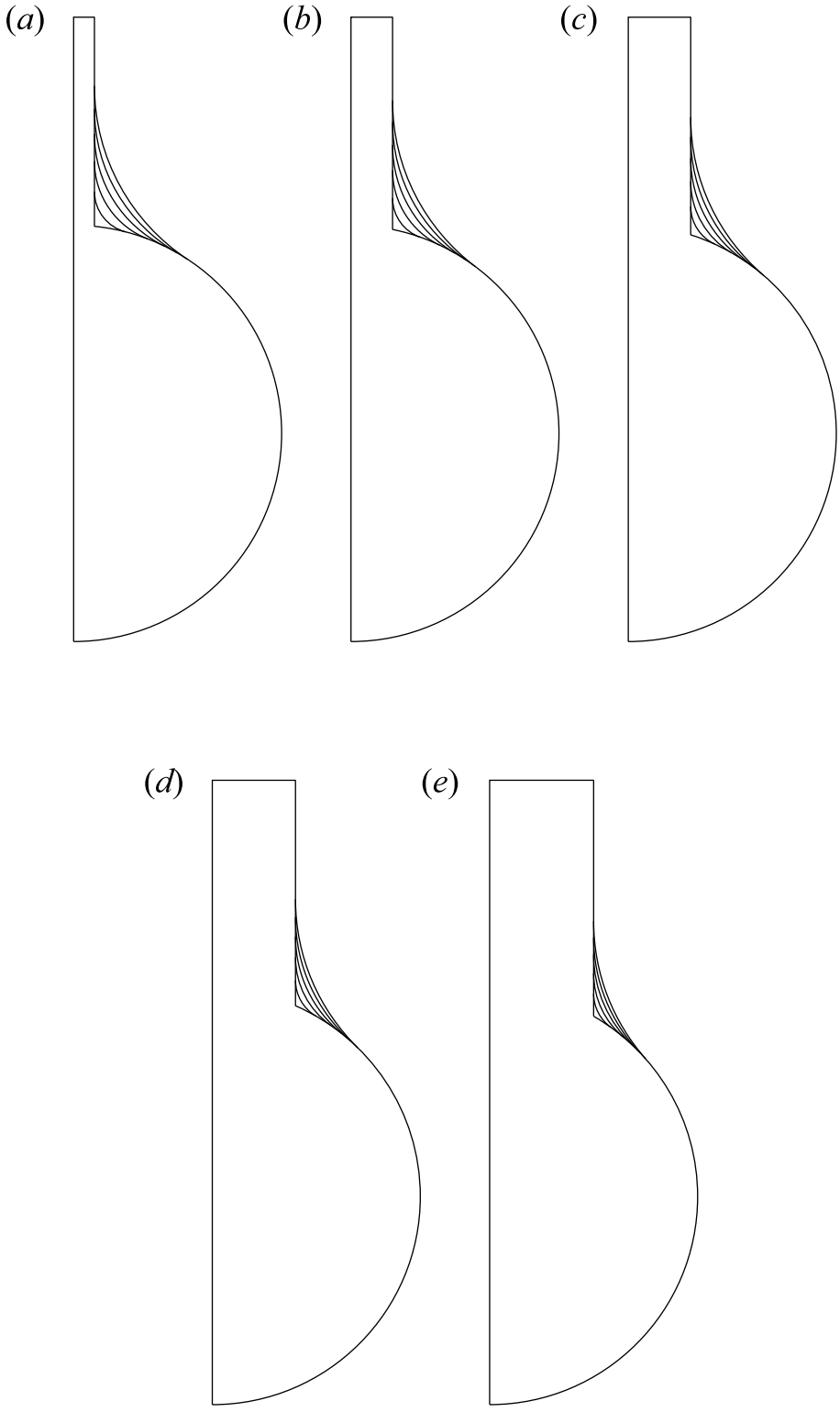

Figure 9: Analysis of the effect of fillet radius in a re-entrant groove (to scale, $\phi = 90°$, $H^* = 2.0$, $H_l^* = 3.0$, $\tau_{lv}^* = 0.0$): (a) $W^*/2 = 0.1$; (b) $W^*/2 = 0.2$; (c) $W^*/2 = 0.3$; (d) $W^*/2 = 0.4$; (e) $W^*/2 = 0.5$.

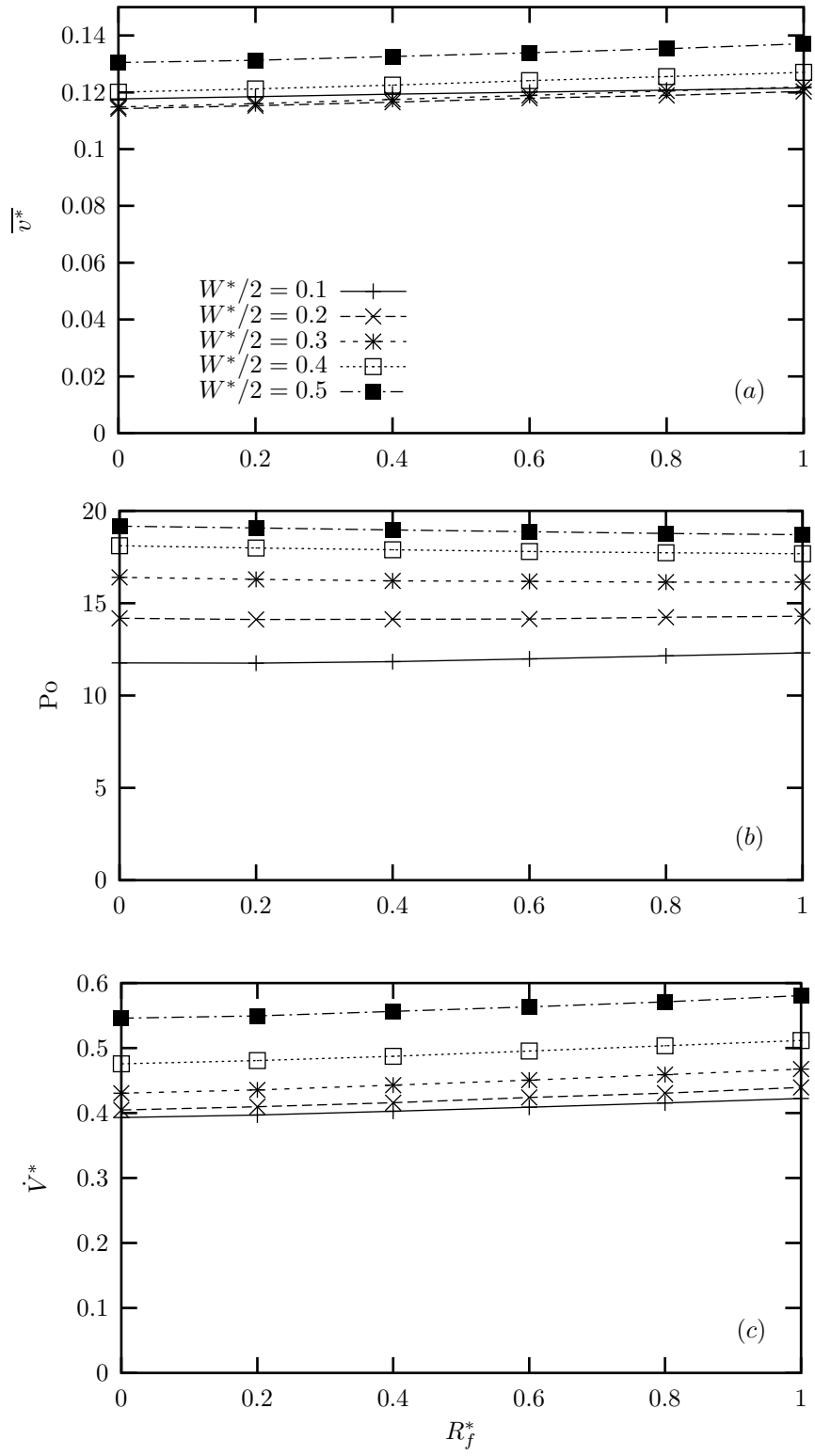

Figure 10: Variation of the flow variables with fillet radius ($\phi = 90°$, $H^* = 2.0$, $H_l^* = 3.0$, $\tau_{lv}^* = 0.0$): (a) Mean velocity; (b) Poiseuille number; (c) Volumetric flow rate.

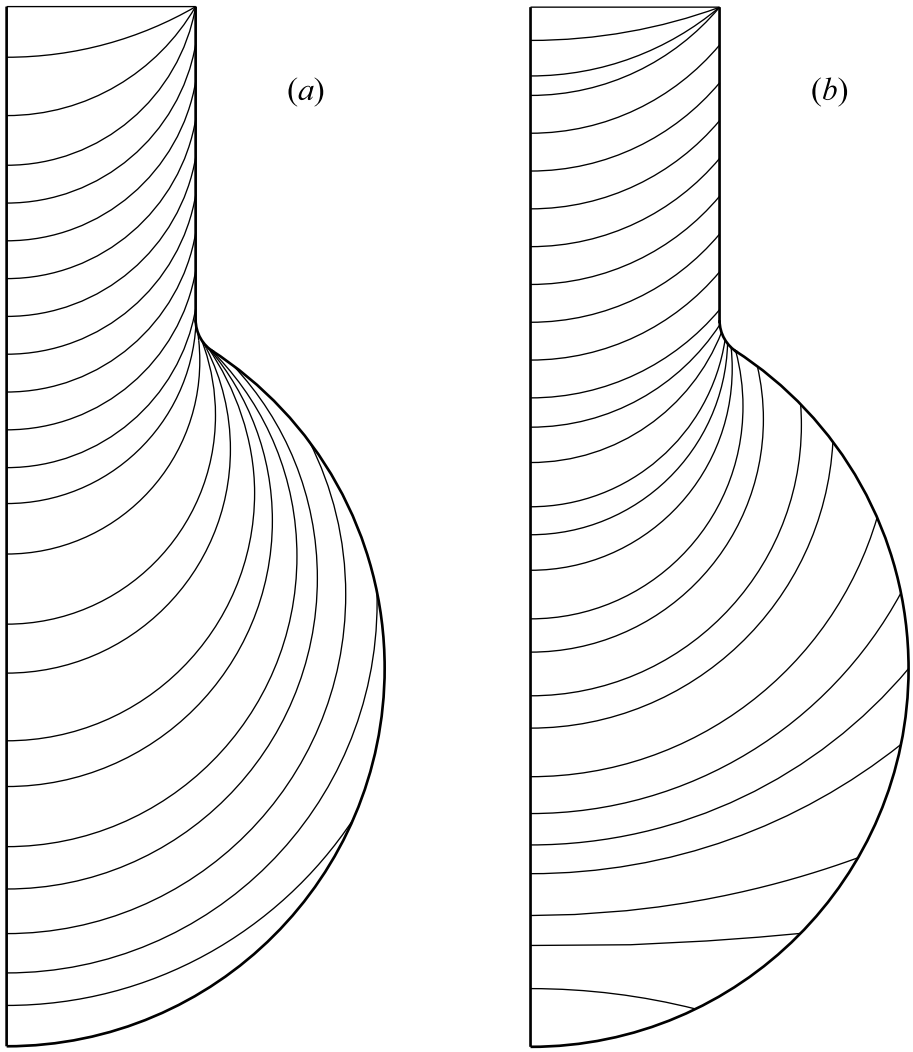

Figure 11: Analysis of liquid fill amount in a re-entrant groove (to scale, $H^* = 1.75$, $W^*/2 = 0.5$, $R_f^* = 0.1$): (a) $\phi_0 = 10°$; (b) $\phi_0 = 40°$.

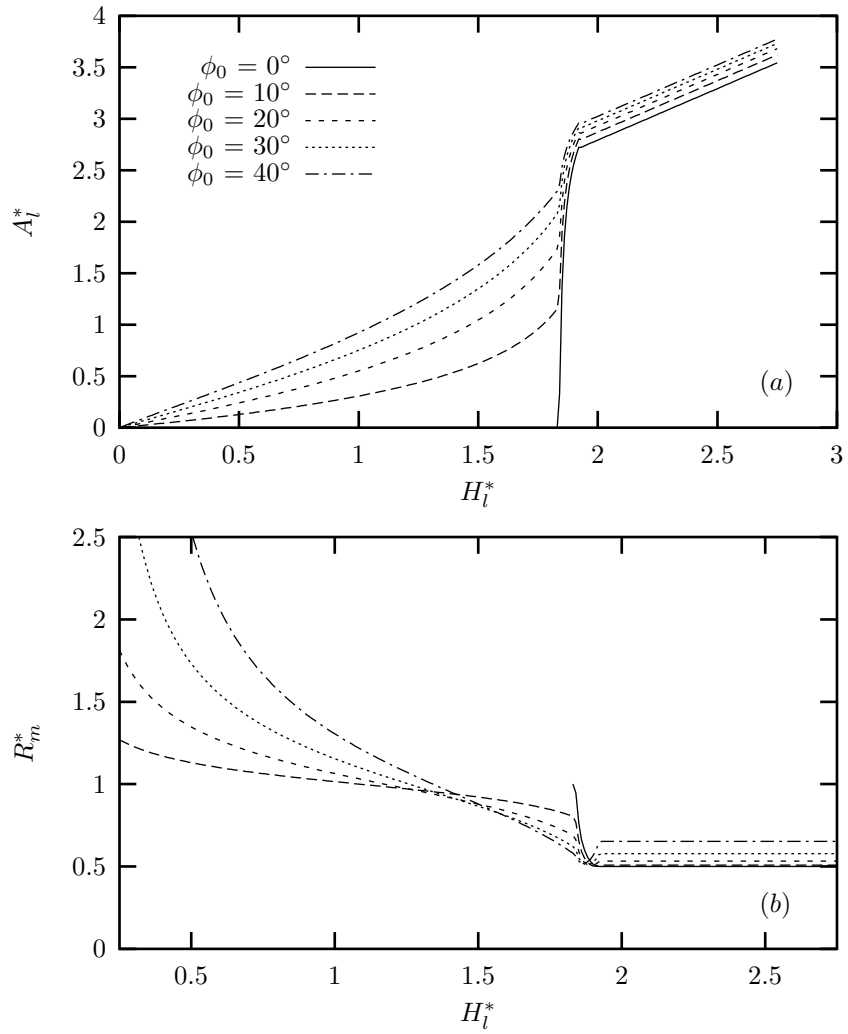

Figure 12: Variation of geometric properties with meniscus attachment point ($H^* = 1.75$, $W^*/2 = 0.5$, $R_f^* = 0.1$): (a) Liquid cross-sectional area; (b) Meniscus radius.

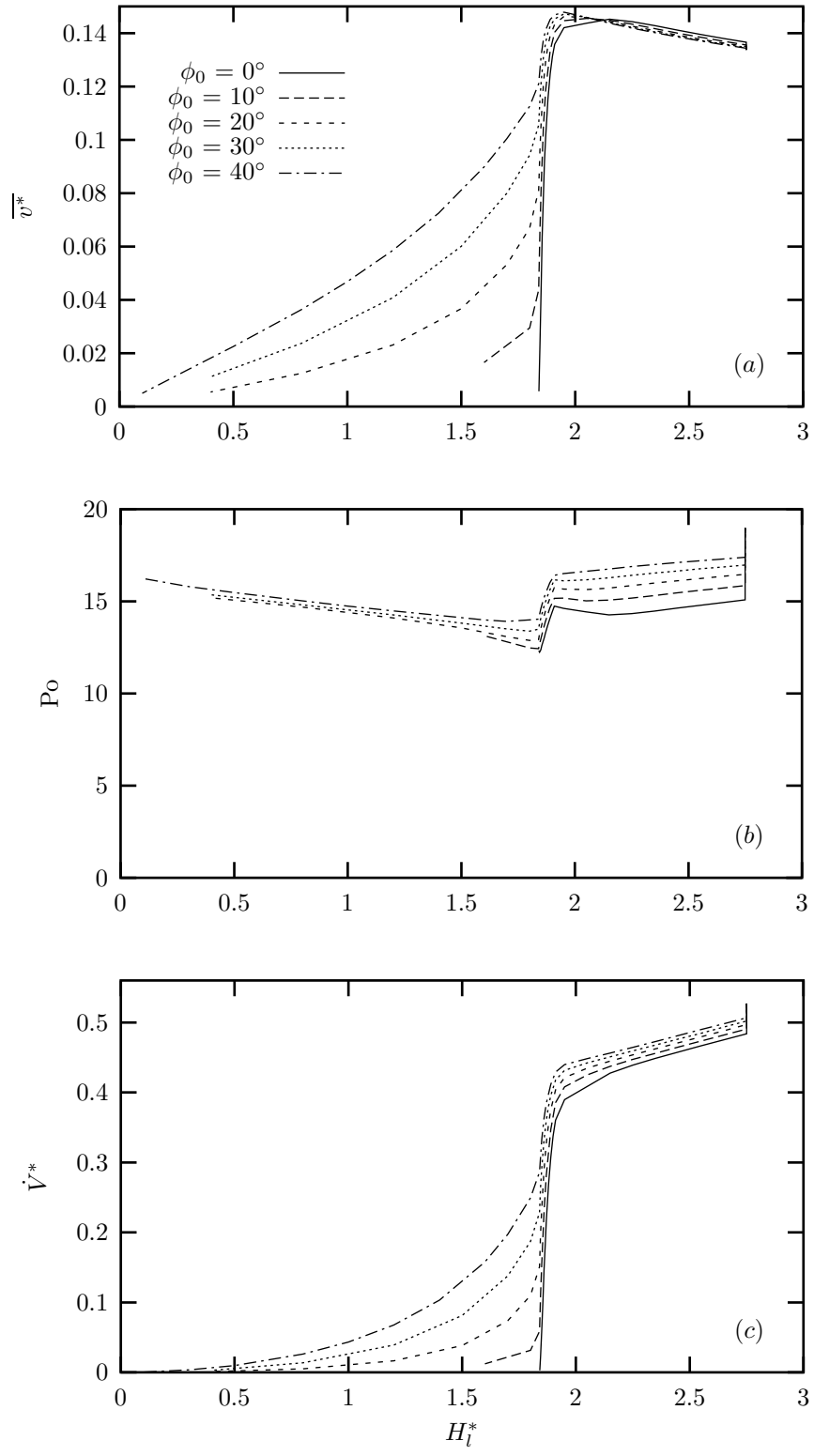

Figure 13: The effect of meniscus attachment point on the flow variables for the re-entrant groove ($H^* = 1.75$, $W^*/2 = 0.5$, $R_f^* = 0.1$, $\tau_{lv}^* = 0.0$): (a) Mean velocity; (b) Poiseuille number; (c) Volumetric flow rate.

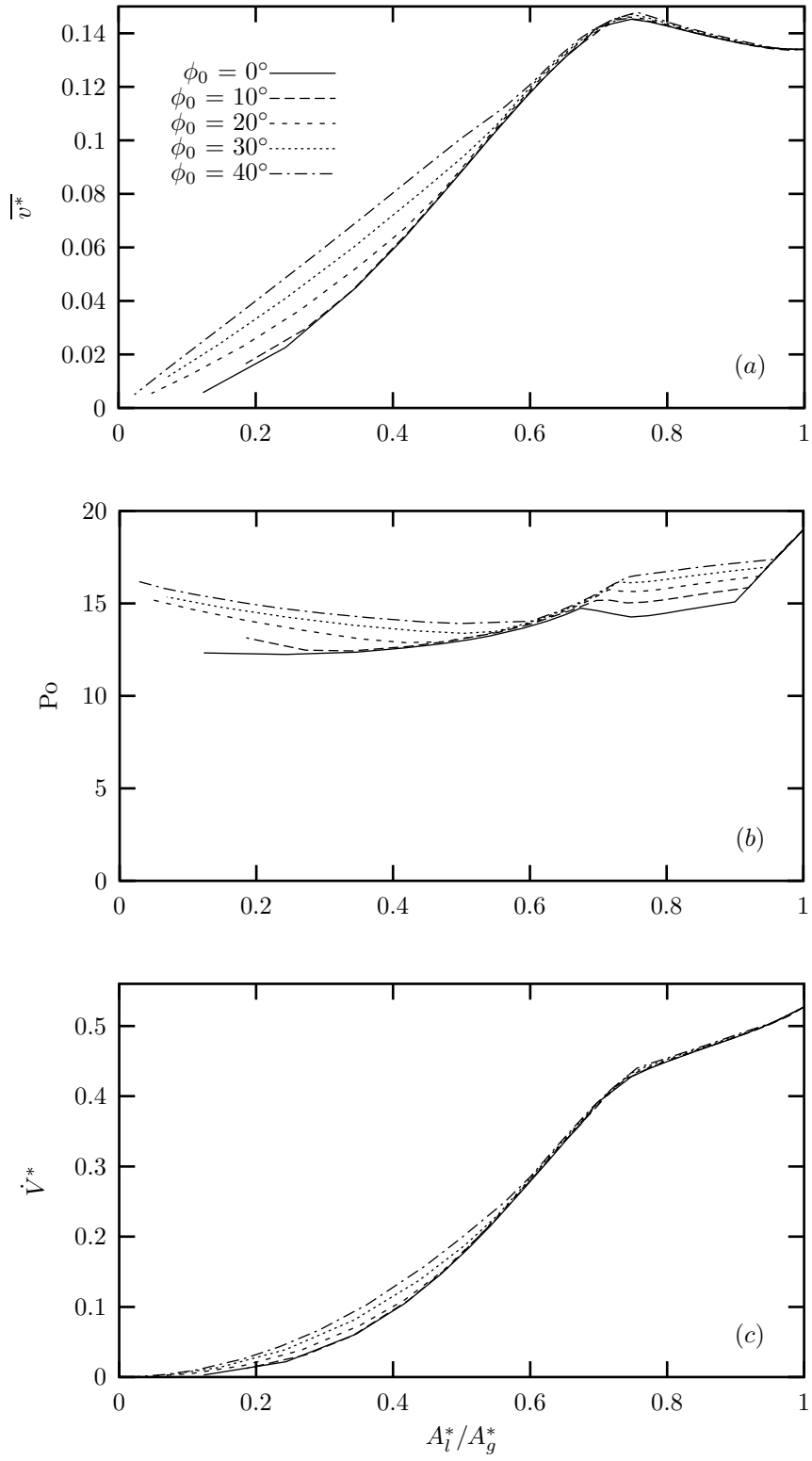

Figure 14: The effect of liquid fill amount on the flow variables for the re-entrant groove ($H^* = 1.75$, $W^*/2 = 0.5$, $R_f^* = 0.1$, $\tau_{lv}^* = 0.0$): (a) Mean velocity; (b) Poiseuille number; (c) Volumetric flow rate.

Table 1: Specifications of the re-entrant groove heat pipe.

Evaporator length	$L_e = 15.2 \times 10^{-2}$ m
Adiabatic length	$L_a = 8.2 \times 10^{-2}$ m
Condenser length	$L_c = 15.2 \times 10^{-2}$ m
Radius of the heat pipe vapor space	$R_v = 8.59 \times 10^{-3}$ m
Radius of the circular portion of the groove	$R = 0.8 \times 10^{-3}$ m
Groove height	$H = 1.4 \times 10^{-3}$ m
Slot half-width	$W/2 = 0.4 \times 10^{-3}$ m
Number of grooves	$N_g = 15$
Operating temperature	$T_{\text{sat}} = 60°\text{C}$

The capillary pressure for an axial groove is

$$\Delta p_{\text{cap,max}} = \frac{\sigma}{R_m} \tag{33}$$

For a circular cross section heat pipe with uniform heat input and output along the lengths of the evaporator and condenser, respectively, the pressure drop in the vapor is

$$\Delta p_v = \frac{8\mu_v L_{\text{eff}} \dot{Q}_t}{\pi \rho_v h_{\text{fg}} R_v^4} \tag{34}$$

The Poiseuille number of the vapor flow was modelled as laminar flow within a smooth tube with a circular cross section ($\text{Po}_v = 16$).

The pressure drop in the liquid was found using the dimensionless mean velocity determined by the numerical model.

$$dp_l = -\left(\frac{\mu_l \overline{v}_l}{R^2 \overline{v^*}}\right) dy \tag{35}$$

For a constant heat flux in both the evaporator and condenser sections, eqn. (35) can be integrated to determine the total pressure drop in the re-entrant groove.

$$\Delta p_l = L_{\text{eff}} \left(\frac{\mu_l \overline{v}_{l,\max}}{R^2 \overline{v^*}}\right) \tag{36}$$

The maximum liquid velocity in a groove is in the adiabatic section.

$$\overline{v}_{l,\max} = \frac{\dot{Q}_g}{\rho_l A_l h_{\text{fg}}} \tag{37}$$

A closed-form solution for the capillary limit of a heat pipe with re-entrant axial grooves and no body forces is

$$\dot{Q}_{\text{cap}} = \frac{\sigma h_{\text{fg}}}{R_m L_{\text{eff}}} \left(\frac{\mu_l}{N_g R^4 \rho_l \dot{V}^*} + \frac{8\mu_v}{\pi \rho_v R_v^4}\right)^{-1} \tag{38}$$

Equation (38) was evaluated using the results of the analysis for the effect of groove fill amount for the heat pipe presented in Table 1. The properties of water and ethanol were found by evaluating the temperature-dependent equations provided by Faghri [18]. The capillary limit heat transport is shown versus the meniscus attachment point in Fig. 15 and versus the groove fill amount in Fig. 16.

When the groove is completely full with $\phi = 90°$, the capillary limit is zero due to the infinite meniscus radius. The capillary limit quickly increases as the contact angle decreases to the minimum meniscus contact angle, at which point $\dot{Q}_{\text{cap}}$ begins to fall off due to the decrease in volumetric flow rate. The maximum value of the capillary limit is greater for smaller values of meniscus contact angle, as expected. Fig. 15 clearly shows that when the liquid recedes into the fillet region, the heat transport decreases rapidly, which demonstrates the importance of proper fluid fill amount in this type of heat pipe.

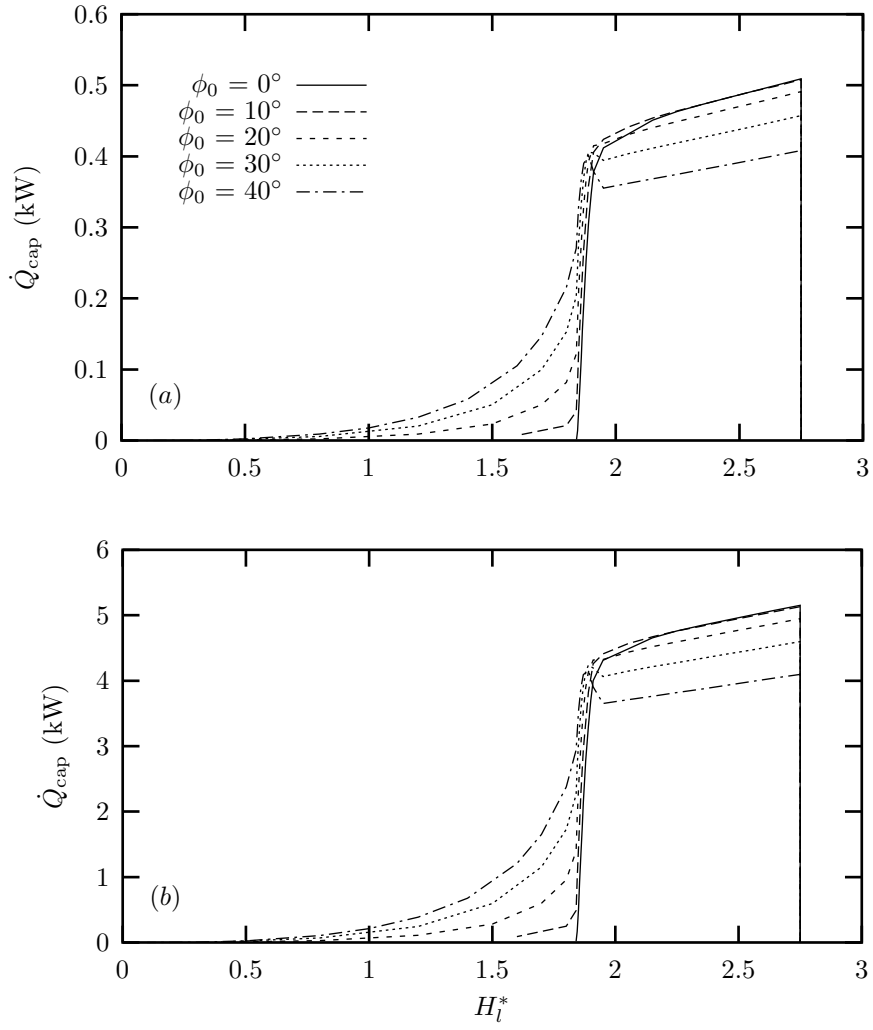

Figure 15: Heat transport versus meniscus attachment point for different values of the minimum meniscus contact angle ($H^* = 1.75$, $W^*/2 = 0.5$, $R_f^* = 0.1$, $\tau_{lv}^* = 0.0$): (a) Ethanol; (b) Water.

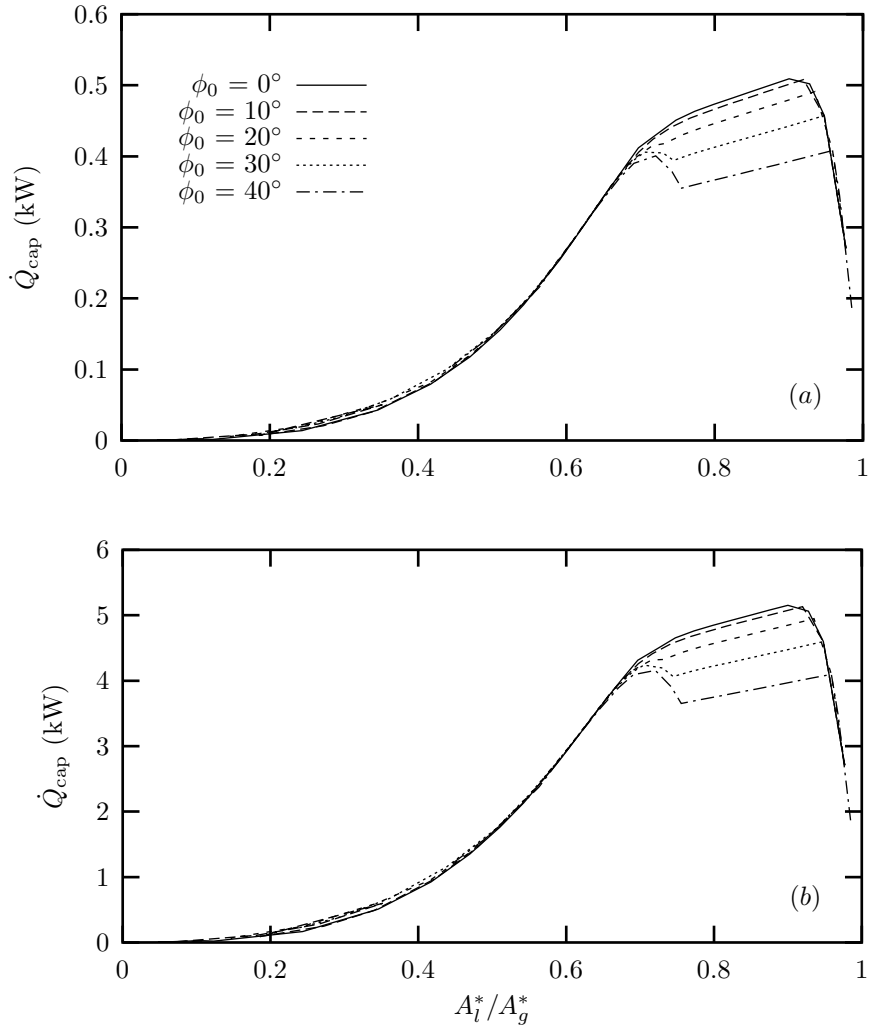

Figure 16: Heat transport versus liquid fill amount for different values of the minimum meniscus contact angle ($H^* = 1.75$, $W^*/2 = 0.5$, $R_f^* = 0.1$, $\tau_{lv}^* = 0.0$): (a) Ethanol; (b) Water.

V. Conclusions

A study has been completed wherein the Poiseuille number, mean velocity, and volumetric flow rate of a liquid in a re-entrant groove have been determined as functions of groove geometry, meniscus contact angle and liquid-vapor shear stress. In addition, the effects of meniscus recession were discussed and related to the performance of a heat pipe with axial re-entrant grooves. The main conclusions from this study are as follows:

1. Using the finite element model it was possible to apply the countercurrent shear stress boundary condition normally to the liquid meniscus, which gave more accurate results than those obtained by a finite difference model used by one of the previous researchers (Thomas et al. [16], [17]). The error in the Poiseuille number was found to be up to 14% for trapezoidal grooves and sinusoidal grooves. Also, the computer resources required by the finite element model were much less as compared to the finite difference model.

2. The results of the parametric analysis of the re-entrant groove showed that the Poiseuille number was greatly affected by the liquid-vapor shear stress, groove height, and slot half-width, but was relatively insensitive to the fillet radius. Significant errors in the prediction of the liquid pressure drop in an axial re-entrant groove would be induced by assuming that the Poiseuille number was the same as that for a smooth tube (Po = 16). Therefore, it is recommended that the Poiseuille number be evaluated using the methodology outlined in this manuscript, particularly if countercurrent vapor flowing above the meniscus imparts a significant shear stress on the liquid meniscus.

3. The volumetric flow rate for slot half-widths of $W^*/2 \leq 0.3$ approached a fairly constant value of $\dot{V}^*$ $= 0.41$ for the groove height ranging from $1.0 \leq H^* \leq 4.0$ for a full groove with no shear stress at the meniscus. This fact could be important to heat pipe designers for use with the analytical prediction of the capillary limit provided in eqn. (38).

4. The capillary limit heat transfer attained a maximum value in the slot region and decreased dramatically as the meniscus receded into the circular region of the re-entrant groove. This shows the critical nature of the fluid fill amount in heat pipes with axial re-entrant grooves.

References

[1] Harwell, W., Kaufman, W., and Tower, L., Re-Entrant Groove Heat Pipe, *Proc. 12th AIAA Thermophysics Conf.*, pp. 131-147, AIAA Paper No. 77-773 (1977).

[2] Dubois, M., van Oost, S., Bekaert, G., and Supper, W., High Capacity Grooved Heat Pipes, *Proc. 4th European Symposium on Space Environmental Control Systems*, Florence, Italy, pp. 575-581 (1991).

[3] Dubois, M., Mullender, B., and Supper, W., Space Qualification of High Capacity Grooved Heat Pipes, *Proc. 27th International Conf. on Environmental Systems*, Lake Tahoe, Nevada, SAE Paper No. 972453 (1997).

[4] Alario, J., Haslett, R., and Kosson, R., The Monogroove High-Performance Heat Pipe, AIAA Paper No. 81-1156 (1984).

[5] Alario, J., Monogroove Heat Pipe Radiator Shuttle Flight Experiment: Design, Analysis and Testing, *Proc. 14th Intersociety Conf. on Environmental Systems*, SAE Paper No. 840950 (1984).

[6] Henson, R., *Thermohydraulic Modelling of a Monogroove Heat Pipe Condensor*, Masters Thesis, North Carolina State University, Raleigh, North Carolina (1998).

[7] Brown, R., Kosson R., and Ungar, E., Design of the SHARE II Monogroove Heat Pipe, *AIAA 26th Thermophysics Conference*, AIAA Paper No. 91-1359, June 24-26, (1991).

[8] Schlitt, R., Performance Characteristics of Recently Developed High-Performance Heat Pipes, *Heat Transfer Engineering*, **16**, 44-52, (1995).

[9] Brandt, C., Stephan P., Dubois, M., and Mullender, B., Theoretical Investigation of Advanced Capillary Structures in Grooved Heat Pipe Evaporators for Space Applications, *Proc. 30th Int. Conf. Environmental Systems,* Toulouse, France, SAE Paper No. 2000-01-2319 (2000).

[10] White, F., *Viscous Fluid Flow* (2nd Edn.), McGraw-Hill, New York (1991).

[11] Incropera, F., and DeWitt, D., *Fundamentals of Heat and Mass Transfer* (4th Edn.), Wiley, New York (1996).

[12] Damle, V., *Analysis of Fluid Flow in Axial Re-entrant Grooves with Application to Heat Pipes*, Masters Thesis, Wright State University, Dayton, Ohio (2004).

[13] Shah, R., and London, A., *Laminar Flow Forced Convection in Ducts*, Academic, New York (1978).

[14] DiCola, G., Soluzionne Analitica, Amezzo Della Transformata di Fourier, di un Problema di Fusso in un Canale Rettangolare, *Euratom C.C.R.*, Ispra, Italy, C.E.T.I.S. (1968).

[15] Romero, L., and Yost, F., Flow in an Open Channel, *J. Fluid Mech.* **322**, pp. 109-129 (1996).

[16] Thomas, S., Lykins, R., and Yerkes, K., Fully-Developed Laminar Flow in Sinusoidal Grooves, *ASME J. Fluids Engineering*, **123**, pp. 656-661 (2001).

[17] Thomas, S., Lykins, R., and Yerkes, K., Fully Developed Laminar Flow in Trapezoidal Grooves with Shear Stress at the Liquid-Vapor Interface, *Int. J. Heat Mass Transfer*, **44**, pp. 3397-3412 (2001).

[18] Faghri, A., *Heat Pipe Science and Technology*, Taylor and Francis, Washington, D.C. (1995).

[19] Hopkins, R., Faghri, A., and Khrustalev, D., Flat Miniature Heat Pipes with Micro Capillary Grooves, *ASME J. Heat Transfer*, **121**, pp. 102-109 (1999).

[20] Chi, S., *Heat Pipe Theory and Practice: A Sourcebook,* Hemisphere Publ. Corp., New York (1976).